Nuclear Materials and Energy 24 (2020) 100765

Contents lists available at ScienceDirect

Nuclear Materials and Energy

journal homepage: www.elsevier.com/locate/nme

Diffusion bonding effects on the adhesion of tungsten dust on tungsten surfaces

P. Tolias[a,*], M. De Angeli[b], S. Ratynskaia[a], G. Riva[c], P. Bassani[d], D. Ripamonti[c], A. Nardone[b], M. Pedroni[b], D. Ricci[b]

[a] Space and Plasma Physics – KTH Royal Institute of Technology, Teknikringen 31, 10044 Stockholm, Sweden
[b] Institute for Plasma Science and Technology – Consiglio Nazionale delle Ricerche, via Cozzi 53, 20125 Milan, Italy
[c] Institute of Condensed Matter Chemistry and Energy Technologies – Consiglio Nazionale delle Ricerche, via Cozzi 53, 20125 Milan, Italy
[d] Institute of Condensed Matter Chemistry and Energy Technologies – Consiglio Nazionale delle Ricerche, via Previati 1/E, 23900 Lecco, Italy

ARTICLE INFO

Keywords:
Dust adhesion
Pull-off force measurement
Diffusion bonding
Contact aging
Dust resuspension
Dust collection

ABSTRACT

High temperature excursions have the potential to strongly enhance the room temperature adhesion of tokamak dust. Planar tungsten substrates containing adhered nearly monodisperse spherical tungsten dust have been exposed to linear plasmas and vacuum furnaces. Prolonged thermal treatments of varying peak temperature and constant duration were followed by room temperature adhesion measurements with the electrostatic detachment method. Adhesive forces have been observed to strongly depend on the thermal pre-history, greatly increasing above a threshold temperature. Adhesive forces have been measured up to an order of magnitude larger than those of untreated samples. This enhancement has been attributed to atomic diffusion that slowly eliminates the omnipresent nanometer-scale surface roughness, ultimately switching the dominant interaction from long-range weak van der Waals forces to short-range strong metallic bonding.

1. Introduction

The adhesion of tokamak generated dust on plasma-facing components (PFCs) has been gradually acknowledged to play an important role in plasma-induced dust remobilization [1,2], dust-wall mechanical impacts [3,4], pre-plasma remobilization of ferromagnetic dust [5], dust resuspension during loss-of-vacuum accidents (LOVAs) [6,7], dust collection activities [8,9] & dust removal techniques [10]. This motivated systematic adhesion measurements for micron-sized tungsten dust deposited on tungsten substrates (W-on-W) using the electrostatic detachment method [11–14] and more recently the colloidal probe technique [15]. These experimental investigations have managed to quantify the effect of the dust deposition technique [12], beryllium coating thickness [12], atmospheric contaminants [13], thin oxide layers [14] and surface roughness [15] on the W-on-W adhesion. However, all available fusion relevant measurements have been carried out in room temperature.

Low temperature conditions seem to be appropriate for various tokamak applications such as pre-plasma remobilization, resuspension during LOVAs and dust collection or removal. Nevertheless, dust-PFC contacts should undergo a large number of high temperature excursions during successive tokamak discharges prior to room temperature collection, removal, remobilization or resuspension. In ITER, even after excluding edge-localized modes and slow transient reattachment events, the stationary heat fluxes incident to the divertor vertical targets should be high enough to raise the surface temperatures close to or beyond the W recrystallization range of 1373–1700 K [16–18]. Given the foreseen long ITER pulse durations [19], even limited atomic W diffusion at such temperatures could strengthen the dust-PFC contact and increase the room temperature W-on-W adhesive force by filling the nano-roughness pockets of the interface and leading to diffusion bonding.

The purpose of the present work is to quantify the effect of contact aging under high temperature conditions on the room temperature W-on-W adhesion. This is achieved by prolonged exposures of planar W substrates containing adhered monodisperse W dust to linear plasmas or vacuum furnaces that are followed by room temperature adhesion measurements with the electrostatic detachment method. The experimental sequence aims to mimic the temperature history of dust-PFC contacts that is relevant for the aforementioned tokamak applications. The vacuum furnace exposures allow for robust controlled variations of the sample temperature in an impurity-free environment, whereas linear plasma exposures reproduce tokamak conditions in a more realistic manner. The exposure durations of ~8000 s in furnaces and of

* Corresponding author.
E-mail address: tolias@kth.se (P. Tolias).

https://doi.org/10.1016/j.nme.2020.100765
Received 20 February 2020; Received in revised form 28 May 2020; Accepted 16 June 2020
Available online 27 June 2020

5400 s in linear plasmas were selected to correspond to a respectable fraction of the 55,000 s overall discharge time currently envisaged for the first ITER phase of Fusion Power Operation (FPO-I) [19,20]. The highest steady state sample temperatures of 1303 K reached in the exposures remained safely below the nominal temperatures above which W recrystallization is expected to occur [18].

The manuscript is organized as follows. In Section 2, established theoretical descriptions of adhesion are presented and complications due to surface roughness are discussed. In Section 3, the underlying physics of the electrostatic detachment method are introduced and the technical aspects of the experimental procedure are described. In Section 4, the W-on-W vacuum furnace and linear plasma exposures are presented and the subsequent adhesion measurements are analyzed. In Section 5, a theoretical explanation of the qualitative experimental trends is put forward. In Section 6, future work and implications for ITER are discussed.

2. Theoretical background

The pull-off force is the minimum normal external force that is required to separate two surfaces in close proximity. By definition, the pull-off force is equal in magnitude and opposite in direction to the adhesive force that quantifies the tendency of two surfaces to stick to each other. Herein, these terms shall be used interchangeably. In what follows, we provide a concise presentation of fundamental theoretical descriptions of adhesion focusing on atomically smooth surfaces and also discuss the effects of surface roughness.

The microscopic description of adhesion is only applicable to non-deformable bodies [21]. It is implicitly assumed that the adhesive force stems exclusively from the cumulative interaction between all instantaneously induced and/ or permanent multipoles inside the two contacting bodies. Therefore, primary chemical bonding is neglected and the pull-off force is the opposite of the van der Waals force. For a perfectly spherical body of radius R_d in the proximity of a perfectly planar surface, we simply have [22]

$$F_\mathrm{po}^\mathrm{vdW} = \frac{A}{6z_0^2}R_\mathrm{d}, \tag{1}$$

with $z_0 (\ll R_\mathrm{d})$ the distance of closest approach between the two bodies and A the Hamaker constant. In the case of W-on-W, the closest approach should exceed the range of the metallic bond resulting from electron exchange interactions that are excluded from the van der Waals force [22]. Given the ~0.3 nm range of the metallic bond, we end up with $z_0 = 0.4$ nm [23]. The Hamaker constant is calculated from the non-retarded limit of Lifshitz theory that requires knowledge of the dielectric function of the contacting bodies and the surrounding medium [24–26]. Recent accurate calculations based on the Lifshitz formalism that utilize extended-in-frequency reliable dielectric data without invoking any theoretical simplifications or computational approximations have led to $A = 4.98 \times 10^{-19}$ J for the room temperature W-vacuum-W system [27]. It is worth noting that geometrical roughness effects can be incorporated in microscopic descriptions by considering asperity models of rough surfaces and decomposing the total van der Waals force into contact plus non-contact terms. Such procedure is followed in the Rumpf [28] and Rabinovich models [29].

The macroscopic description of adhesion is applicable to deformable bodies in separations of the order of the lattice parameter [21], *i.e.* in intimate contact. The pull-off force is calculated by the contact mechanics approach and bodies are treated as continuous elastic media [30], implying that plastic as well as viscoelastic effects are neglected. For the perfect sphere - plane system, we have [31–33]

$$F_\mathrm{po}^\mathrm{cma} = \xi_\mathrm{a}\Delta\gamma R_\mathrm{d}, \tag{2}$$

where $(3/2)\pi \leqslant \xi_\mathrm{a} \leqslant 2\pi$ is the adhesiveness parameter [34] that acquires its lower bound within the Johnson-Kendall-Roberts (JKR) theory [35] and acquires its upper bound within the Derjaguin-Muller-Toporov (DMT) theory [36]. The work of adhesion is given by $\Delta\gamma = \gamma_1 + \gamma_2 - \Gamma$, with γ_i the surface energies and Γ the interface energy. In the case of W-on-W at room temperature, we have $\gamma = 4.36$ J/m^2 and $\Gamma \simeq 0$ from first principle calculations [37] and experiments [38]. We note that the adopted surface energy incorporates metallic bonding in an automatic manner [11]. It is worth pointing out that deformation roughness effects can arise due to the existence of different asperity heights, which lead to a competition between the compressive elastic forces exerted by the higher asperities and the adhesive forces exerted by the lower asperities. Such effects can be incorporated in macroscopic descriptions by applying the continuum elastic models to individual micro-contacts and by summing up the respective contributions [39].

The difference between Eqs. (1, 2) is better understood in terms of equivalent surface energies. Within JKR theory, the van der Waals surface energy is given by $\gamma_\mathrm{vdW} = A/(18\pi z_0^2)$ that leads to $\gamma_\mathrm{vdW} \simeq 0.055$J/m^2 for W-on-W at room temperature. The surface energy associated with the metallic bond is nearly 80 times larger than the surface energy associated with van der Waals interactions [22], thus reflecting the relative strengths of the two forces [23]. This is valid for most metals, since $A = (1.8 - 5.3) \times 10^{-19}$ J and $\gamma = 0.5 - 5.9$ J/m^2. Experimental measurements of the pull-off force for metal dust adhered on metal surfaces can be orders of magnitude less than contact mechanics predictions and agree within few factors with van der Waals predictions [11,32,40]. This result has been attributed to the omnipresent surface roughness. As the asperity dimensions begin to exceed the characteristic range of the primary chemical bond, the overall interaction will be progressively dictated by van der Waals forces. The metallic bond decay length should be of the order of few Thomas–Fermi screening lengths that implies a few Ångströms [22,23]. Hence, even a root-mean-square roughness R_q of few nanometers should suffice to switch the dominant interactions.

3. Adhesive force measurements

Experimental techniques that measure the dust-surface adhesive force are generally based on exerting a controlled stepwise increasing separation force until dust mobilization is realized. The *colloidal probe method* of atomic force microscopy (AFM) measures cantilever deflection at the instant of detachment that can be converted into the respective spring force after careful calibration [41,42]. The *centrifugal method* utilizes the centrifugal force arising from a rapidly rotating surface [43,44]. The *electrostatic detachment method* employs the electrostatic force resulting from the interaction between an externally imposed electric field and the contact charge it induces on adhered metallic dust grains [45]. *Hydrodynamic and aerodynamic methods* subject adhered dust to momentum exchange forces induced by laminar or even turbulent fluid flows [46,47]. The *inertial detachment method* takes advantage of surface acceleration induced by shockwaves [48]. The *vibrational method* takes advantage of inertial forces generated by the excitation of high frequency surface vibrations [49,50].

The pull-off force measurements reported in this work are carried out with the electrostatic detachment method. The basic advantage of the method lies in the fact that the dust-loaded substrate constitutes one of the removable electrodes of the device. As a consequence, controlled dust deposition on the substrate can be easily performed by any technique. More important, the dust-loaded substrate can be directly exposed to thermal treatments or plasma loads prior to the measurements. The basic disadvantage of the method concerns the occurrence of dielectric breakdown that imposes a maximum to the externally applied electrostatic field depending on the operating pressure. Given the linear dependence of the adhesive force and the quadratic dependence of the mobilizing force on the dust radius, see Eqs. ()(1)–(3), the method cannot be used to measure the adhesive force for very small dust grains. In what follows, we shall briefly present the operation principle of the method, the main stages of the experimental procedure and the basic aspects of the raw output post-processing. For further details, the reader

is referred to our previous works [11,12].

The device consists of a parallel plate cylindrical capacitor placed in a vacuum chamber ($<5 \times 10^{-4}$ mbar). A dc potential difference is applied between the two electrodes with the dust-loaded substrate acting as the grounded electrode. The resulting normal electrostatic force tends to detach the grains from the substrate. For the perfect sphere-plane system, it is described by the Lebedev formula [51]

$$F_e = k_R E^2 R_d^2 \ (\mu N), \tag{3}$$

where E is the electrostatic field in kV/mm, R_d the dust radius in μm and $k_R = 1.52 \times 10^{-4}$ (μNmm^2)/(kV^2 μm^2). This is the dominant external force acting on dust grains, since dielectrophoretic forces are negligible due to the minimization of fringing effects, capillary forces are weak due to the low pressures, aerodynamic forces during pumping are negligible for geometrical reasons and gravity can be ignored compared to adhesion [12]. The pull-off force F_{po} can thus be indirectly measured by slowly increasing the bias until the detachment condition $F_e \geqslant F_{po}$ is satisfied.

As a result of the omnipresent structural (surface topology), chemical (adsorbates) as well as energetic (monocrystal orientation) heterogeneities [52,53], complete detachment does not occur above a unique electric field strength but partial detachment occurs over an extended range of fields [11,12]. The method essentially provides a measurement of the cumulative distribution function $\Phi(\cdot)$ of the random variable F_{po} [12,13], whose average and spread can be directly computed from the expressions [11–13]

$$\overline{F}_{po} = \sum_{i=1}^{M} \left[\left(\frac{N_i}{N} \right) F_{e,i} \right] / \sum_{i=1}^{M} \left(\frac{N_i}{N} \right), \tag{4}$$

$$\sigma[F_{po}] = \sqrt{\sum_{i=1}^{M} \left[\left(\frac{N_i}{N} \right) (F_{e,i} - \overline{F}_{po})^2 \right] / \sum_{i=1}^{M} \left(\frac{N_i}{N} \right)} \tag{5}$$

with M the number of distinct electrostatic field values, N the total number of adhered dust grains, N_i the number of grains detached by a given E_i applied field and $F_{e,i}$ the sampled value of the pull-off force. The quantity N_i is determined by comparing successive optical images of the sample, whereas the quantity $F_{e,i}$ is determined from the Lebedev formula evaluated at the average adhered dust radius $\overline{R}_d$, *i.e.* $F_{e,i} = k_R E_i^2 \overline{R}_d^2$. The denominator is not necessarily unity, since dielectric breakdown can occur prior to detachment of all adhered dust grains [11,12]. Its inclusion is intended to compensate for the lack of strong field measurements. However, Eqs. (4, 5) are accurate only when a low dust fraction remains adhered post breakdown.

In the present measurements, two nearly monodisperse W dust batches (of 4.5 μm and 7 μm nominal radius) were meshed out with high precision electroformed nickel sieves and ultrasonic cells from a wide 2–13μm population supplied by TEKNA Advanced Materials. The W powder was characterized by high sphericity, high purity, low porosity and excellent electrical conductivity [12]. The planar W substrates were sandpaper polished in order to ensure similar rms roughness characteristics, $R_q \sim 30$ nm as measured by a surface profiler (KLA-Tencor P15, KLA-Tencor Corporation) with a 0.2 nm resolution. Standard pre-cleaning techniques were followed, *i.e.* gross polishing with turpentine followed by ultrasonic baths in turpentine & acetone for several minutes. The W dust was then adhered to the substrates in a controlled manner with gravity-assisted deposition [12]. The dust-loaded substrates (W-on-W) were initially subject to an electrostatic field of 6 kV/mm capable of detaching dust clusters but unable to detach isolated dust grains. Such a pre-treatment nearly eliminated agglomerates that have the potential to strongly contaminate measurements. The W-on-W samples were afterwards exposed to the vacuum furnaces or the linear plasma device.

The exposed samples constituted the bottom electrode of the high-voltage system. A 6 kV potential difference was first applied and maintained constant for several minutes. Afterwards, the vacuum was broken, the bottom electrode was dismounted and the number of mobilized dust grains N_i was counted with the aid of an optical microscope. The same procedure was followed with a slightly higher bias, until all dust was removed or dielectric breakdown was realized. With 0.5–1 mm electrode spacings and 6–25 kV potential biases, applied fields varied within 6–50 kV/mm.

Experimental errors in the determination of the pull-off force can originate from uncertainties in particle counting (negligible), the applied potential bias (negligible), the electrode spacing (significant) and dust radius (dominant). The 25 μm uncertainty in electrode spacing leads to ± 2.5% (6–25 kV/mm fields) or ± 5.0% (25–50 kV/mm fields) uncertainty in the sampled pull-off force $F_{e,i}$. In the nominal 4.5 μm population, the actual mean radius is 4.4 μm with a ± 0.4 μm standard deviation that leads to ± 18.2% uncertainty in $F_{e,i}$. In the nominal 7.0 μm population, the actual mean radius is 7.2 μm with a ± 0.8 μm standard deviation leading to ± 22.2% uncertainty in $F_{e,i}$.

4. Experimental results

4.1. Vacuum furnace exposures

The *high temperature exposures* $\gtrsim$ 500 °C were carried out in a high vacuum furnace (Centorr Series 2100). This prevented W oxidation that has the potential to strongly affect adhesion and whose rates have been documented to rapidly increase above 400 °C [54,55]. The vacuum system features a rotary pump and a diffusive pump allowing us to reach a base vacuum of $<2 \times 10^{-5}$ mbar. W-on-W samples were placed on a Mo sheet inside the furnace chamber. On the other hand, the *low temperature exposures* $\lesssim$ 400 °C were carried out in a vacuum furnace featuring a two-stage rotary pump that achieved a vacuum grade of $\lesssim$ 0.2 mbar.

In both furnaces, thermal treatment was initiated after chamber evacuation. Heating rates in terms of Kelvin-per-hour were kept steady up to a maximum temperature that was maintained for a respectable duration. It is worth emphasizing that the heating rate varied between samples in a manner that ensured that the total heating time remained constant regardless of the targeted temperature. The heat supply was then terminated and the chamber underwent cooling under vacuum conditions. Finally, when the room temperature was approached after nearly an hour of cooling, the pump was stopped and the sample was extracted. The adhesion measurements were performed soon after each furnace exposure. Overall, 15 W-on-W samples have been subject to 8 distinct heating schemes. The exposure conditions of each sample are detailed in Table 1.

A total of 10 furnace exposed W-on-W samples featured nearly monodisperse 7.2 μm dust (subject to all the 8 distinct heating schemes) and a total of 5 furnace exposed W-on-W samples featured nearly monodisperse 4.4 μm dust (subject to 4 distinct heating schemes). Systematic room temperature measurements originally reported in Ref. [12] were included in the datasets, serving as reference points. The direct output of the electrostatic detachment method, concerning the mobilized dust fraction as a function of the applied electrostatic field strength, has been illustrated in Figs. 1a,b for the 7.2 μm and the 4.4 μm batches, respectively. Regardless of the dust radius, the W-on-W adhesive force is nearly independent of the low target temperatures (300–600 K) and becomes rapidly stronger as the targeted temperature further increases (700–1300 K).

Unfortunately, owing to the large adhesion increase at the highest targeted temperatures $\gtrsim$ 900 K, the maximum electrostatic field reached prior to the dielectric breakdown only suffices to mobilize a small percentage of the originally adhered dust grains. Consequently, the average value and the spread of the pull-off force cannot be reliably extracted for these exposures. Nevertheless, a conservative estimate of the lower bound of the average pull-off force has been attempted based on the maximum applied electrostatic field that cannot lead to dust mobilization. Important figures-of-merit that quantify adhesion are

Table 1
Summary of **vacuum furnace exposures** of W substrates loaded with spherical W dust adhered by gravity-assisted deposition. A total of 15 polished planar W substrates containing 2 different nearly monodisperse W dust populations were subject to the thermal treatment.

Maximum sample temperature	Vacuum grade (mbar)	Number of samples exposed	Sample heating rate (K/hour)	Temperature rise time (hours)	Temperature hold time (min)	Total heating time (hours)	Total heating time (sec)
1303 K	$<2\times10^{-5}$	2	500	2.0	15	2.25	8100
1103 K	$<2\times10^{-5}$	1	400	2.0	15	2.25	8100
1003 K	$<2\times10^{-5}$	1	350	2.0	15	2.25	8100
903 K	$<2\times10^{-5}$	1	300	2.0	15	2.25	8100
803 K	$<2\times10^{-5}$	2	250	2.0	15	2.25	8100
674 K	~ 0.2	4	190	1.9	15	2.15	7740
573 K	~ 0.2	2	140	2.0	15	2.25	8100
503 K	~ 0.2	2	105	2.0	15	2.25	8100

provided in Table 2.

The average pull-off force has been plotted as a function of the spherical dust radius in Fig. 2 and compared with the van der Waals force. Close to room temperature (300–600 K), the pull-off force is approximately constant (within the experimental uncertainties) and nearly equal to the van der Waals force. From roughly 700 K and up to 1300 K, the pull-off force begins to strongly increase with the maximum sample temperature largely surpassing the van der Waals value.

4.2. Linear plasma exposures

GyM is a medium-flux steady-state linear plasma machine. The device and the sample introduction system have been described in Refs. [56–58]. The parameters of the deuterium plasma were measured with a Langmuir probe only at the column center. The exposed W-on-W samples were negatively biased with respect to the plasma and their surface normal was oriented parallel to the incident plasma flux. All discharges were similar; the plasma density varied within $n = (4.9 - 6.5)\times10^{10}\,\mathrm{cm}^{-3}$, the electron temperature varied within $T_e = 7.0$–7.5 eV, the plasma potential varied within $V_p = 15$–20 V and the ion fluence varied within $F_i = (2.2\text{–}6.1)\times10^{24}\,\mathrm{m}^{-2}$. The exposure time was $t_{exp} = 90$ min and the sample bias $V_b = -400$ V. The ions were nearly mono-energetic ($T_i \sim 0.1$ eV) with an incident energy of $E_{inc} = e(V_p - V_b)$. Overall, 5 W-on-W samples were exposed to 5 plasma discharges. The exact exposure conditions of each sample are detailed in Table 3.

In all discharges, the final temperature of the sample holder ranged within 629–643 K. As expected from the similar plasma parameters and the identical sample bias, the surface temperatures should be similar in all the exposures. The plasma column parameters have a strong radial dependence which leads to a radially dependent heat flux and surface temperature distribution. Since plasma measurements could only be performed at the column center, estimates of the spatial variations of the incident plasma heat flux were not possible. As a result, thermal analysis could not be carried out to compute the surface temperature variations. Thus, the holder temperature is the only indicator of the unknown radially-varying plasma-facing side temperature.

Owing to the strong negative bias with respect to the plasma, the incident ion energy exceeds the D on W physical sputtering threshold of $E_{th} \simeq 230$ eV [59]. In our exposures, the normal incidence sputtering yield varied within $Y_{D\to W}(E_{inc}) = (8.1\text{–}8.5)\times10^{-4}$ according to the Eckstein-Preuss empirical formula [59,60]. This simple estimate neglects sputtering by oxygen impurities, self-sputtering by promptly ionized W atoms and the D_2 plasma content [13]. It results to an erosion depth, $s = [F_i Y_{D\to W}(E_{inc}) m_{at}]/\rho_m$ with m_{at} the W atomic mass and ρ_m the W mass density, that varies within 30–80 nm between exposures.

In spite of the strong negative bias, the plasma pressure is several orders of magnitude lower than the W yield strength and the nominally compressive ion-induced forces are several orders of magnitude lower than adhesive forces. This is a direct result of the relatively low plasma densities. As a consequence, during the GyM plasma exposures, the state of the dust-surface contact is not affected by particle flux loads but only by heat flux loads similar to the vacuum furnace exposures. The only difference lies in the possibility of surface roughness modifications induced by sputtering and of near-surface chemistry modifications induced by sputtering or thermal desorption of contaminants. However, the dust-substrate contact area is optically shielded from the incident ions. It is, thus, reasonable to assume that such effects are negligible.

The exposures labelled as #1, #2 took place in the first experimental campaign, whereas the exposures labelled as #3, #4, #5 took place in the second campaign. It should be pointed out that the W-on-W sample alignment along the vessel axis (that coincides with the plasma beam center where the particle and heat fluxes become maximum) has been problematic in the first campaign. The issue was resolved in the second campaign, where the W-on-W sample position was corrected by 6 mm. Hence, the dust loaded region is subject to much stronger heat fluxes and reaches higher surface temperatures in exposures #3, #4, #5.

A total of 4 GyM exposed samples featured spherical nearly

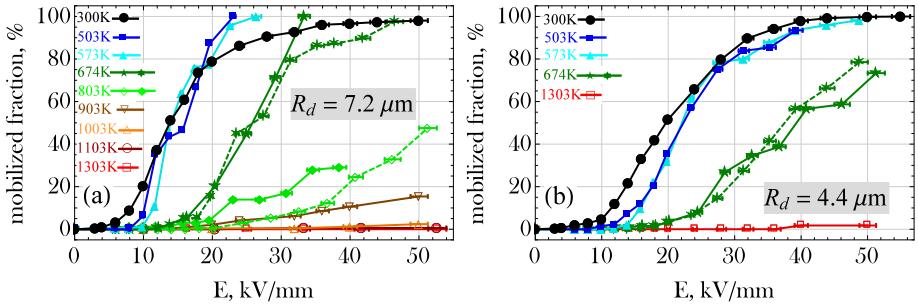

Fig. 1. Electrostatic detachment measurements on furnace exposed samples; the mobilized dust percentage as a function of the applied electrostatic field for monodisperse spherical W dust of (a) 7.2 μm, (b) 4.4 μm. The W samples are coined after the peak temperature reached during exposure, see Table 1. The horizontal error bars (field uncertainty) stem from the 25 μm uncertainty in the inter-electrode spacing of $d = 0.5$ mm or 1.0 mm. The room temperature measurements are characterized by much better statistics that are manifested in the smoother curves and by the mobilization of a very small dust fraction below 6 kV/mm due to the lack of field pre-treatment to remove agglomerates.

Table 2
Summary of the pull-off force measurements performed with the electrostatic detachment method on the **furnace exposed samples**. The symbol (†) signifies that the quoted measurements correspond to the particle-weighted averages of two identical exposures. The symbols (☆) and (◇) signify that the quoted room temperature measurements correspond to the values originally reported in Ref. [12] after re-scaling from $R_d = 7.41\ \mu m$ to $R_d = 7.2\ \mu m$, from $R_d = 4.47\ \mu m$ to $R_d = 4.4\ \mu m$. The designation "N/A" refers to measurements where the spread of the pull-off force could not be extracted, due to the fact that most grains remained attached to the substrate after the dielectric breakdown.

Maximum sample temperature	Average dust radius (μm)	Number of isolated dust grains	Average pull-off force (μN)	Pull-off force spread (μN)	Mobilized percentage 20 kV/mm	Mobilized percentage 40 kV/mm	Mobilized percentage at breakdown
1303 K	7.2	180	>25.3	N/A	0%	0%	0%
1103 K	7.2	168	>21.8	N/A	0%	0.6%	0.6%
1003 K	7.2	247	>15.3	N/A	0%	1.2%	2.4%
903 K	7.2	292	>12.6	N/A	2.1%	10.6%	15.4%
803 K(†)	7.2	369	11.04	4.23	2.2%	26.6%	39.3%
674 K(†)	7.2	366	6.51	3.13	17.5%	94.3%	98.6%
573 K	7.2	166	2.26	1.21	77.7%	100%	100%
503 K	7.2	164	2.20	1.09	87.2%	100%	100%
300 K(☆)	7.2	714	2.70	2.95	78.9%	96.6%	98.1%
1303 K	4.4	1024	>8.58	N/A	0%	0%	1.8%
674 K(†)	4.4	1366	4.17	1.87	3.37%	56.5%	76.6%
573 K	4.4	572	2.08	1.39	32.0%	93.5%	98.3%
503 K	4.4	322	1.87	1.08	35.7%	93.5%	93.5%
300 K(◇)	4.4	3112	1.72	1.33	51.6%	97.9%	99.9%

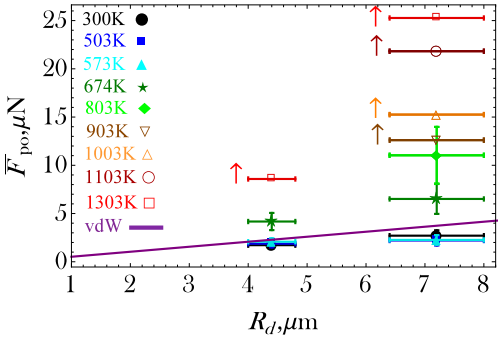

Fig. 2. The average value of the W-on-W adhesive force as function of the dust radius for different vacuum furnace heating schemes. The vertical error bars in the 300 K, 503 K, 573 K, 674 K, 803 K results stem from the electrode spacing and dust size uncertainties. The vertical arrows accompanying the 903 K, 1003 K, 1103 K, 1303 K results indicate that the quoted value is a lower bound estimate. Naturally, experimental uncertainties could not be estimated for the latter exposures. The van der Waals result for the room-temperature W-on-W adhesive force, see Eq. (1), has also been plotted for comparison.

monodisperse 4.4 μm dust, while a single GyM exposed sample featured nearly monodisperse 7.2 μm dust. Systematic room temperature measurements originally reported in Ref.[12] were included in the datasets, serving again as reference points. The direct output of the electrostatic detachment method, concerning the mobilized dust percentage as a function of the applied electrostatic field strength, has been illustrated in Fig. 3a and b for the 4.4 μm and 7.2 μm batches, respectively. Regardless of the dust size, W-on-W adhesion becomes stronger compared to the room-temperature measurements. In case of a premature dielectric breakdown, a conservative estimate of the lower bound of the average pull-off force has been again attempted. As expected, given the misalignment and different surface temperatures, the extracted average pull-off force for exposures #1, #2 is much smaller than the pull-off force estimates for #3, #4. Important figures-of-merit that quantify adhesion are provided in Table 4.

The average pull-off force has been plotted as a function of the spherical dust radius in Fig. 4 and compared with the theoretical van der Waals force. In the misaligned exposures, the measured pull-off force becomes 50–65% larger than the room-temperature van der Waals force; an increase exceeding the combined experimental uncertainty. On the other hand, in properly aligned exposures, the measured pull-off force becomes from several factors up to an order of magnitude larger than the room-temperature van der Waals force.

It is worth mentioning that, after their exposure to the GyM plasma and the electrostatic detachment device, the W-on-W samples were inspected by a scanning electron microscope (SEM). The SEM images revealed the presence of nearly circular footprints whose location coincided with the dust deposition sites and whose radius was approximately equal to the adhered dust radius. These footprints have been attributed to the physical sputtering that erodes the entire substrate surface with the exception of the small areas that are geometrically shadowed by the adhered dust grains. In fact, atomic force microscopy confirmed that the footprint height varied within 80–105 nm consistent with our rough estimate of the erosion depth. See also Fig. 5 for the image of a typical footprint. The same AFM analysis revealed that the substrate surface roughness is not drastically affected by the exposure to the GyM plasma. For instance, the rms roughness R_q increases from

Table 3
Summary of **linear plasma exposures** of W substrates loaded with spherical W dust adhered by gravity-assisted deposition. The symbol (†) signifies exposures that took place in the first GyM experimental campaign, where the dust loaded region of the W-on-W sample acquired sub-nominal surface temperatures owing to misalignment issues. A total of 5 polished planar W substrates that contained 2 different nearly monodisperse W dust populations were exposed in the GyM medium-flux device.

GyM plasma exposure	Plasma potential (V)	Plasma density (cm^{-3})	Electron temperature (eV)	Ion fluence (m^{-2})	Final holder temperature (K)	Exposure time (min)	Applied sample bias (V)
#1(†)	20	5.1×10^{10}	7.5	2.2×10^{24}	633	90	−400
#2(†)	20	4.9×10^{10}	7.5	2.2×10^{24}	638	90	−400
#3	16	6.5×10^{10}	7.0	6.1×10^{24}	633	90	−400
#4	16	6.1×10^{10}	7.1	6.0×10^{24}	629	90	−400
#5	15	6.1×10^{10}	7.0	6.0×10^{24}	643	90	−400

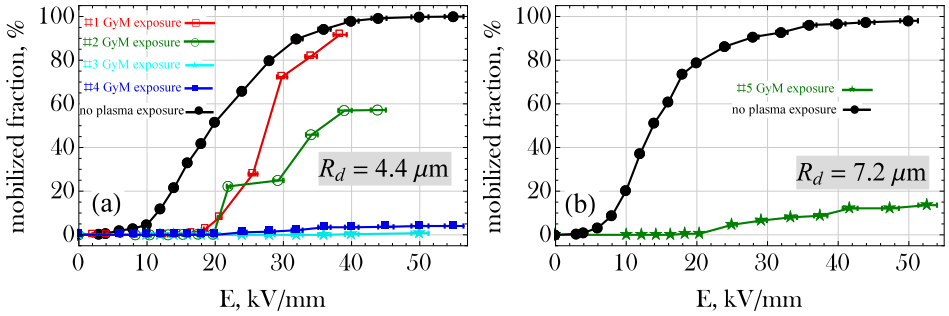

Fig. 3. Electrostatic detachment measurements on **plasma exposed samples**; the mobilized dust percentage as a function of the applied electrostatic field for monodisperse spherical W dust of (a) 4.4 μm, (b) 7.2 μm. See Table 3 for the exposure details. The horizontal error bars (applied field uncertainty) stem from the 25 μm uncertainty in the inter-electrode spacing of d = 0.5 mm or 1.0 mm. The room temperature measurements are characterized by much better statistics that are manifested in the smoother curves and by the mobilization of a very small dust fraction below 6 kV/mm due to the lack of field pre-treatment to remove agglomerates. It should be pointed out that in the pull-off force measurements that were carried out on the W-on-W samples exposed in the first experimental campaign (#1, #2), dielectric breakdowns and arcs occurred at lower electrostatic fields than expected, limiting their strength at ~ 40 kV/mm compared to the standard ~ 50 kV/mm.

Table 4
Summary of the pull-off force measurements performed with the electrostatic detachment method on the **plasma exposed samples**. The designation "N/A" refers to measurements where the spread of the pull-off force could not be extracted, since most dust grains remained attached to the substrate after the occurrence of dielectric breakdown. The designation "no plasma" refers to the room temperature measurements on samples never exposed to plasma that were originally reported in Ref. [12], after re-scaling from R_d = 4.47 μm to R_d = 4.4 μm and from R_d = 7.41 μm to R_d = 7.2 μm. The symbol (†) signifies exposures that took place in the first GyM experimental campaign, where the dust loaded region of the W-on-W sample acquired sub-nominal surface temperatures owing to misalignment issues.

GyM plasma exposure	Nominal dust radius (μm)	Number of isolated dust grains	Average pull-off force (μN)	Pull-off force spread (μN)	Mobilized percentage 20 kV/mm	Mobilized percentage 40 kV/mm	Mobilized percentage at breakdown
#1(†)	4.4	998	2.60	0.82	7.9%	91.7%	91.7%
#2(†)	4.4	964	2.82	1.22	0.3%	56.9%	57.2%
#3	4.4	663	>9.38	N/A	0%	0.3%	0.8%
#4	4.4	1039	>8.90	N/A	0%	3.5%	4.0%
no plasma	4.4	3112	1.72	1.33	51.6%	97.9%	99.9%
#5	7.2	412	>4.92	N/A	0.5%	12.1%	13.6%
no plasma	7.2	714	2.70	2.95	78.9%	96.6%	98.1%

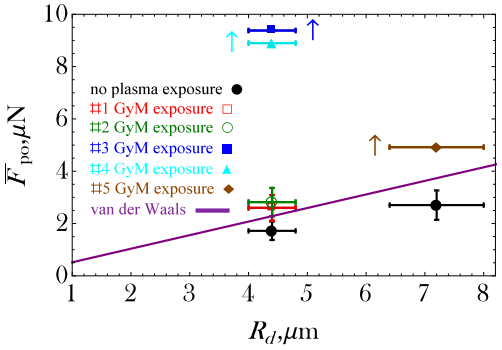

Fig. 4. The average value of the measured W-on-W pull-off force as a function of the dust radius for the GyM linear plasma exposures. The vertical error bars in the results of the #1 and #2 exposure stem from the electrode spacing and dust size uncertainties. The vertical arrows accompanying the results of the #3, #4 and #5 exposure indicate that the quoted value is a lower bound estimate. Naturally, experimental uncertainties could not be estimated for the latter exposures. The van der Waals result for the room-temperature W-on-W adhesive force, see Eq. (1), has also been plotted for comparison.

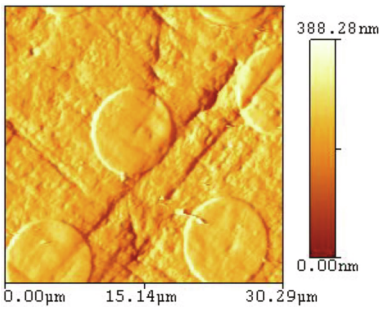

Fig. 5. AFM image of the circular substrate footprints that are generated around the dust deposition sites and are revealed after the electrostatic detachment of adhered dust. The areas of the substrate that are shadowed by dust cannot be physically sputtered by the normally directed ion flux, in contrast to the remaining areas. This facilitates a straightforward local measurement of the erosion depth.

19 nm to 25 nm for the #1 substrate and the same metric increases from 22 nm to 46 nm for the #3 substrate.

5. Discussion

In both vacuum furnace and linear plasma exposures, the external forces acting on the adhered dust grains are unable to cause plastic deformation or viscoelastic flattening at the contact sites. The observed increase of the W-on-W adhesion with the final sample temperature (for a constant exposure time) can be safely attributed to atomic W diffusion, provided that possible complications due to surface adsorbates and bulk impurities are negligible. In our previous investigations focusing on the effect of atmospheric contaminants [13], room temperature measurements led to effective Hamaker constants within (2.22–3.93) × 10^{-19} J that is roughly half the theoretical 4.98 × 10^{-19} J Lifshitz value [27], while surface analysis revealed a low content of native oxides in both the W dust and substrates involved. Moreover,

pure metals are characterized by the strongest van der Waals interactions [23] with W possessing one of the highest Hamaker constants amongst metals [61]. Thus, even though the dissociation of atmospheric contaminants and bulk diffusion of trace impurities during the thermal treatments cannot be excluded, they could be responsible for an up-to-twofold adhesion increase and not for the order of magnitude increase inferred from our measurements.

The following physical interpretation of the observed adhesion enhancement is proposed. *At relatively low temperatures*, mass transfer should remain low and the role of diffusion (if any) should be restricted to slowly decreasing the dimensions of the surface asperities. As a consequence, geometrical and deformation effects due to surface roughness might decrease possibly leading to a small increase of adhesion towards the nominal van der Waals magnitude. *At relatively high temperatures*, material migration should rapidly increase and atomic W diffusion in the interfacial voids should eliminate most of the nanoroughness pockets. As a consequence, adhesion should be mainly controlled by metallic bonding which implies a large adhesive force increase towards the nominal JKR magnitude that is nearly 80 times larger. *At even higher temperatures*, but still below the W recrystallization range and much lower than the W melting point, the adhesion can only slightly change due to small contact area changes. Overall, for a constant exposure time, the W-on-W adhesive force as function of the steady state temperature should strongly resemble a sigmoid curve, whose low temperature asymptote is slightly lower than the van der Waals result and whose high temperature asymptote is very close to the JKR result.

In Fig. 6, the measured W-on-W adhesive force normalized by the room temperature van der Waals value has been plotted versus the maximum vacuum furnace temperature. Our adhesion measurements after linear plasma exposures have not been included in the figure, since the temperature of the plasma facing side remained unknown. For both dust sizes, the experimental results are consistent with our qualitative theoretical discussion. Unfortunately, **(i)** the upper asymptotic region is obscured because of the inability of our present electrostatic mobilization set-up to reliably measure very high adhesive forces owing to the occurrence of dielectric breakdown, **(ii)** the lower asymptotic region is not properly resolved since possible slight adhesion changes are overshadowed by the experimental uncertainties and uneven particle statistics. Nevertheless, the transition between the asymptotes is well captured.

We shall coin this mechanism as diffusion bonding after the eponymous solid-state welding technique that is based on the same physical principle [62]. The primary difference with the welding technique lies in the fact that in the latter high temperatures are complemented with respectable compressive stresses that are high enough to speed up the joining process but still too low (compared to the material yield strength) to cause excessive plastic deformation [62].

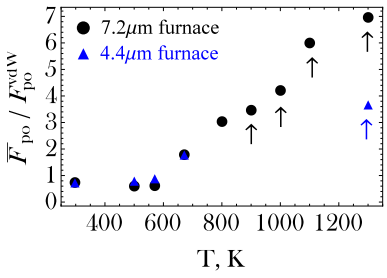

Fig. 6. The average value of the measured W-on-W pull-off force for the vacuum furnace exposures as a function of the maximum temperature reached for two monodisperse spherical dust populations. The average pull-off force for each of the two sizes has been normalized by the respective value of the room temperature van der Waals force, see Eq. (1). The vertical arrows that point towards the 903 K, 1003 K, 1103 K and 1303 K results indicate that the quoted value is a lower bound estimate.

It is worth pointing out that there have been very few room temperature adhesion measurements after thermal treatment [63–67]. To our knowledge, the complete sigmoid curve has only been traced once in the literature, namely in the centrifugal method measurements performed by Polke with micron-sized spherical gold dust adhered onto planar gold surfaces [63]. We should emphasize that adhesion measurements that are carried out at high temperatures, *i.e.* during the plateau of the thermal treatment, should be expected to result in much smaller adhesion forces than adhesion measurements that are carried out at room temperature, *i.e.* after sample cooling [63]. This reflects the difference between the enhanced mobility of the hot near-surface atoms compared to the low diffusion rates of cold atoms that are frozen in void-free interfaces. We should also stress that, since diffusion is the most likely candidate for the observed enhancement, the W-on-W adhesive force should depend on the shape of temperature pulse and not only on its peak and total duration.

The strong temperature dependence of atomic W diffusion is reflected in the Arrhenius form of the W diffusivity, whose exact values are determined by the number of possible diffusion channels, their activation energies and their relative strengths [68–71]. It might seem unrealistic that W self-diffusion becomes relevant at such low temperatures compared to the W melting point of 3695 K and the definite answer can only be given by numerical modelling of the dust-surface contact area evolution that lies beyond the scope of the present work. Concerning the transition region and the high temperature asymptote of the sigmoid curve, the long duration of the thermal treatment as well as the proximity to the recrystallization temperature range should make diffusion effective. In addition, solid-state diffusion bonding of W surfaces with EUROFER97 steel surfaces has been successfully realized at temperatures around 1000 K, albeit under the influence of compression stresses of the order of few tens of MPa [72]. On the other hand, concerning the low temperature asymptote of the sigmoid curve, small changes in the adhesive force could also be explained by the gradual diffusion or desorption of surface contaminants and impurities that are capable of altering the van der Waals interactions [13,66].

6. Summary, future work and ITER implications

Monodisperse spherical W dust populations were adhered to planar polished W substrates with the aid of gravity assisted deposition. W-on-W samples were subject either **(i)** to extended thermal treatments of varying peak temperature but constant waveform in vacuum furnaces, or **(ii)** to prolonged steady state exposures to the deuterium plasmas of the GyM medium-flux linear device. Exposures were followed by room temperature adhesion measurements performed with the electrostatic detachment method. In both cases, analysis revealed that adhesive force modifications are mainly governed by temperature pulse characteristics. Thus, we have focused on the more controlled vacuum furnace exposures of constant 2 h pulse rise times and 15 min plateau durations.

The measured average pull-off force was observed to strongly increase at high peak furnace temperatures. For the constant temperature waveform described above, the pull-off force remains nearly constant within 300–700 K, strongly increases around 700–800 K and keeps increasing up to 1300 K. At 1300 K, W-on-W adhesive forces become at least an order of magnitude larger than those measured in untreated room-temperature samples. The increase of the adhesive force has been attributed to contact strengthening owing to diffusion bonding. At low temperatures or short exposures, microscopic material migration slowly fills the nanometer-scale interfacial voids leading to inappreciable adhesive force changes. At high temperatures or long exposures, self-diffusion is ultimately capable of eliminating surface roughness. This is accompanied by a dominant attraction switch from the van der Waals forces to metallic bonding interactions that nominally manifests itself as a nearly two orders of magnitude adhesion enhancement.

Unfortunately, the occurrence of dielectric breakdown at high

electrostatic field strengths prevented us from measuring adhesion after thermal treatments of plateau temperatures above 900 K, where only lower bound estimates were possible. This present set-up limitation can be overcome without having to abandon the electrostatic detachment method. Two strategies will be considered in future work. **(i)** Owing to operation at the left side of the Paschen minimum, for a constant electrode distance, reduction of the operating pressure will lead to a strong increase of the breakdown voltage and thus to stronger electrostatic fields prior to dielectric breakdown. **(ii)** Owing to the linear dependence of the adhesive force on the dust radius as well as the quadratic dependence of the Lebedev separation force on the dust radius, for given breakdown electrostatic fields, the electrostatic detachment method can measure substantially larger adhesion enhancements for larger dust grains. Therefore, it should be beneficiary to focus on larger spherical dust and such batches are commercially available.

Future work will also focus on more controlled and better diagnosed plasma exposures. In the Magnum-PSI linear plasma device, the radial profiles of the plasma density as well as electron temperature can be measured close to the exposed samples by means of Thomson scattering [73] and the surface temperature profiles can be extracted by an infrared camera in combination with multi-wavelength pyrometer [74]. Such experiments would allow for a direct comparison between the vacuum furnace exposures and the plasma exposures.

The present results are relevant for dust resuspension during LOVAs, dust collection activities and dust removal techniques. Experimental facilities measuring dust LOVA resuspension rates under ITER relevant conditions need to generate realistic dust-PFC contacts and numerical codes dedicated to predictive LOVA modelling need to consider such a strong adhesion enhancement. In addition, ongoing tests of the efficiency of ITER dust collection and removal techniques would also need to include dust-PFC contacts that have been subject to prolonged thermal treatments. To be more specific, the observed dependence of the W-on-W adhesive force on the thermal pre-history (contact aging or adhesion hysteresis) together with the significant adhesion enhancement at high temperatures suggest that ITER W dust might gradually become unmobilizable as it accumulates during machine operation. Consequently, the risk of resuspension of a significant amount of W dust during LOVAs might be much lower than currently predicted. However, the degree of risk reduction strongly depends on whether the majority of generated W dust will reside on the hot divertor surfaces or will amass on the cold divertor floor, which is currently unknown. On the other hand, W dust collection and removal activities might need to be frequently planned, otherwise their efficiency might be undermined by contact strengthening.

Finally, extrapolation of the present results for beryllium (Be) dust adhered on tungsten surfaces, whose viability has been suggested by recent experiments [12], leads to adhesion enhancements up to a factor of 60, given the 4.13×10^{-19} J Hamaker constant [27] and 5.65 J/m^2 work of adhesion for the Be-W contact [75]. It should be noted though that complications might arise due to intermetallic compound formation [76]. Be droplets generated in ITER by mitigated major disruptions and vertical displacement events have been predicted to accumulate as re-solidified dust in specific areas of the W divertor [77]. Extrapolation of our results implies that such Be dust would also be hard to collect or resuspend once contact strengthening sets in.

CRediT authorship contribution statement

P. Tolias: Conceptualization, Methodology, Formal analysis, Writing - original draft, Writing - review & editing, Visualization, Project administration. **M. De Angeli:** Investigation, Resources, Supervision. **S. Ratynskaia:** Conceptualization, Project administration, Funding acquisition. **G. Riva:** Investigation. **P. Bassani:** Investigation. **D. Ripamonti:** Investigation. **A. Nardone:** Investigation. **M. Pedroni:** Investigation. **D. Ricci:** Investigation.

Declaration of Competing Interest

The authors declare that they have no known competing financial interests or personal relationships that could have appeared to influence the work reported in this paper.

Acknowledgments

This work has been carried out within the framework of the EUROfusion Consortium and has received funding from the Euratom research and training programme 2014–2018 & 2019–2020 under grant agreement No 633053. The views and opinions expressed herein do not necessarily reflect those of the European Commission. The authors gratefully acknowledge Giambattista Daminelli, Monica De Angeli and Nicola Bennato for technical assistance.

References

[1] P. Tolias, S. Ratynskaia, M. De Angeli, G. De Temmerman, et al., Plasma Phys. Control. Fusion 58 (2016) 025009 .
[2] S. Ratynskaia, P. Tolias, I. Bykov, D. Rudakov, et al., Nucl. Fusion 56 (2016) 066010 .
[3] A. Shalpegin, F. Brochard, S. Ratynskaia, P. Tolias, et al., Nucl. Fusion 55 (2015) 112001 .
[4] P. Tolias, S. Ratynskaia, A. Shalpegin, L. Vignitchouk, et al., Nucl. Mater. Energy 12 (2017) 524.
[5] M. De Angeli, E. Lazzaro, P. Tolias, S. Ratynskaia, et al., Nucl. Fusion 59 (2019) 106033 .
[6] S. Peillon, A. Roynette, C. Grisolia, F. Gensdarmes, Fusion Eng. Des. 89 (2014) 2789.
[7] F. Feuillebois, F. Gensdarmes, T. Gelain, Fusion Eng. Des. 153 (2020) 111500 .
[8] S. Ratynskaia, H. Bergsåker, B. Emmoth, A. Litnovsky, et al., Nucl. Fusion 49 (2009) 073010 .
[9] M. Balden, N. Endstrasser, P.W. Humrickhouse, V. Rohde, et al., Nucl. Fusion 54 (2014) 073010 .
[10] L.B. Begrambekov, A.N. Voityuk, A.M. Zakharov, J. Phys. Conf. Ser. 748 (2016) 012004 .
[11] G. Riva, P. Tolias, S. Ratynskaia, G. Daminelli, et al., Nucl. Mater. Energy 12 (2017) 593.
[12] P. Tolias, G. Riva, M. De Angeli, S. Ratynskaia, et al., Nucl. Mater. Energy 15 (2018) 55.
[13] P. Tolias, M. De Angeli, G. Riva, S. Ratynskaia, et al., Nucl. Mater. Energy 18 (2019) 18.
[14] S. Peillon, M. Sow, C. Grisolia, F. Miserque, et al., J. Electrostat. 88 (2017) 111.
[15] S. Peillon, A. Autricque, M. Redolfi, C. Stancu, et al., J. Aerosol Sci. 137 (2019) 105431 .
[16] T. Hirai, S. Panayotis, V. Barabash, C. Amzallag, et al., Nucl. Mater. Energy 9 (2016) 616.
[17] J.P. Gunn, S. Carpentier-Chouchana, F. Escourbiac, T. Hirai, et al., Nucl. Fusion 57 (2017) 046025 .
[18] G. De Temmerman, T. Hirai, R.A. Pitts, Plasma Phys. Control. Fusion 60 (2018) 044018 .
[19] R.A. Pitts, X. Bonnin, F. Escourbiac, H. Frerichs, et al., Nucl. Mater. Energy 20 (2019) 100696 .
[20] ITER Technical Report ITR-18-003, The ITER Research Plan within the Staged Approach (2018).
[21] D. Tabor, J. Colloid Interface Sci. 58 (1977) 2.
[22] J.N. Israelachvili, Intermolecular and Surface Forces, Academic Press, New York, 2011.
[23] L.-H. Lee, Fundamentals of Adhesion, Springer Science, New York, 1991.
[24] I.E. Dzyaloshinskii, E.M. Lifshitz, L.P. Pitaevskii, Sov. Phys. Usp. 4 (1961) 153.
[25] V.A. Parsegian, Van der Waals forces, Cambridge University Press, Cambridge, 2006.
[26] D.B. Hough, L.R. White, Adv. Colloid Interface Sci. 14 (1980) 3.
[27] P. Tolias, Fusion Eng. Des. 133 (2018) 110.
[28] H. Rumpf, Particle Technology, Chapman & Hall, London, 1990.
[29] Y.I. Rabinovich, J.J. Adler, A. Ata, R.K. Singh, B.M. Moudgil, J. Colloid Interface Sci. 232 (2000) 10.
[30] K.L. Johnson, Contact Mechanics, Cambridge University Press, Cambridge, 1985.
[31] B. Cappella, G. Dietler, Surf. Sci. Rep. 34 (1999) 1.
[32] H.-J. Butt, B. Cappella, M. Kappl, Surf. Sci. Rep. 59 (2005) 1.
[33] D. Maugis, J. Colloid Interface Sci. 150 (1992) 243.
[34] F.L. Leite, C.C. Bueno, A.L. Da Roź 1, E.C. Ziemath, O.N. Oliveira Jr., Int. J. Mol. Sci. 13 (2012) 12773.
[35] K.L. Johnson, K. Kendall, A.D. Roberts, Proc. R. Soc. A 324 (1971) 301.
[36] B. Derjaguin, V.M. Muller, Y.P. Toporov, J. Colloid Interface Sci. 53 (1975) 314.
[37] L. Vitos, A.V. Ruban, H.L. Skriver, J. Kollár, Surf. Sci. 411 (1998) 186.
[38] G. Czack, G. Kirschstein, W. Kurtz, F. Stein, Tungsten: Gmelin Handbook of Inorganic and Organometallic Chemistry vol A4, Springer, Berlin, 1993.
[39] K.N.G. Fuller, D. Tabor, Proc. R. Soc. A 345 (1975) 327.

[40] L.O. Heim, S. Ecke, M. Preuss, H.-J. Butt, J. Adhesion Sci. Technol. 16 (2002) 829.
[41] D.M. Schaefer, M. Carpenter, B. Gady, R. Reifenberger, et al., J. Adhesion Sci. Technol. 9 (1995) 1049.
[42] L.-O. Heim, J. Blum, M. Preuss, H.-J. Butt, Phys. Rev. Lett. 83 (1999) 3328.
[43] H. Krupp, Adv. Colloid Interface Sci. 1 (1967) 111.
[44] D.F.St. John, D.J. Montgomery, J. Appl. Phys. 42 (1971) 663.
[45] D.W. Cooper, H.L. Wolfe, Aerosol Sci. Technol. 12 (1990) 508.
[46] J. Visser, J. Colloid Interface Sci. 34 (1970) 26.
[47] S. Matsusaka, H. Masuda, Aerosol Sci. Technol. 24 (1996) 69.
[48] S. Wanka, M. Kappl, M. Wolkenhauer, H.-J. Butt, Langmuir 29 (2013) 16075.
[49] B.V. Derjaguin, A.D. Zimon, Kolloid. Zh. 23 (1961) 544.
[50] K. Hein, T. Hucke, M. Stintz, S. Ripperger, Part. Part. Syst. Charact. 19 (2002) 269.
[51] N.N. Lebedev, I.P. Skalskaya, Sov. Phys. Tech. Phys. 7 (1962) 268.
[52] K. Cooper, A. Gupta, S. Beaudoin, J. Colloid Interface Sci. 234 (2001) 284.
[53] M. Götzinger, W. Peukert, Langmuir 20 (2004) 5298.
[54] A. Warren, A. Nylund, I. Olefjord, Int. J. Refract. Met. Hard Mater. 14 (1996) 345.
[55] J. Habainy, S. Iyengar, K.B. Surreddi, Y. Lee, Y. Dai, J. Nucl. Mater. 506 (2018) 26.
[56] G. Granucci, D. Ricci, S. Alocci, B. Baiocchi et al., in: Proc. 36th EPS Conference on Plasma Physics, June 29–July 3 2009, Sofia, Bulgaria, ECA, vol. 33E, 2009.
[57] D. Ricci, D. Iraji, A. Cremona, I. Furno et al., in: Proc. 39th EPS Conference on Plasma Physics, 2–6 July 2012, Stockholm, Sweden, ECA, vol. 36F, 2012.
[58] R. Caniello, A. Uccello, F. Ghezzi, D. Minelli, et al., Nucl. Mater. Energy 10 (2017) 9.
[59] R. Behrisch, W. Eckstein, Sputtering by particle bombardment, Springer-Verlag, Berlin, 2007.
[60] W. Eckstein, R. Preuss, J. Nucl. Mater. 320 (2003) 209.
[61] P. Tolias, Non-retarded room temperature Hamaker constants between elemental metals, arXiv:2003.00571v2.
[62] N.F. Kazakov, Diffusion Bonding of Materials, Mir Publishers, Moscow, 1985.
[63] S. Berbner, F. Löffler, Powder Technol. 78 (1994) 273.
[64] L. Kuipers, M.S. Hoogeman, J.W.M. Frenken, Surf. Sci. 340 (1995) 231.
[65] G. Toikka, G.M. Spinks, H.R. Brown, Langmuir 17 (2001) 6207.
[66] H. Kamiya, A. Kimura, T. Yokoyama, M. Naito, G. Jimbo, Powder Technol. 127 (2002) 239.
[67] S.J. Antony, W. Hoyle, Y. Ding, Granular Materials: Fundamentals and Applications, The Royal Society of Chemistry, Cambridge, 2004.
[68] G. Ehrlich, F.G. Hudda, J. Chem. Phys. 44 (1966) 1039.
[69] E.G. Seebauer, C.E. Allen, Prog. Surf. Sci. 49 (1995) 265.
[70] G. Antczak, G. Ehrlich, Surf. Sci. Rep. 62 (2007) 39.
[71] L. Bukonte, T. Ahlgren, K. Heinola, J. Appl. Phys. 115 (2014) 123504 .
[72] W.W. Basuki, J. Aktaa, J. Nucl. Mater. 459 (2015) 217.
[73] H.J. van der Meiden, R.S. Al, C.J. Barth, A.J.H. Donné, et al., Rev. Sci. Intrum. 79 (2008) 013505 .
[74] T.W. Morgan, A. Vertkov, K. Bystrov, I. Lyublinski, et al., Nucl. Mater. Energy 12 (2017) 210.
[75] L. Vignitchouk, P. Tolias, S. Ratynskaia, Plasma Phys. Control. Fusion 56 (2014) 095005 .
[76] S. Ratynskaia, P. Tolias, M. De Angeli, D. Ripamonti, et al., Nucl. Mater. Energy 17 (2018) 222.
[77] L. Vignitchouk, S. Ratynskaia, P. Tolias, R.A. Pitts, et al., Nucl. Fusion 58 (2018) 076008 .